EFDA–JET–PR(13)41

P. Jacquet, V. Bobkov, L. Colas, A. Czarnecka, E. Lerche, M.-L. Mayoral, I. Monakhov, D. Van-Eester, S. Brezinsek, M. Brix, A-L. Campergue, P. Drewelow, M. Graham, C.C. Klepper, A. Meigs, D. Milanesio, J. Mlynar, T. Pütterich, A. Sirinelli and JET EFDA contributors

ICRF Heating in JET During Initial Operations with the ITER-Like Wall

ICRF Heating in JET During Initial Operations with the ITER-Like Wall

P. Jacquet[1], V. Bobkov[2], L. Colas[3], A. Czarnecka[4], E. Lerche[5], M.-L. Mayoral[1,6], I. Monakhov[1], D. Van-Eester[5], S. Brezinsek[7], M. Brix[1], A-L. Campergue[8], P. Drewelow[2], M. Graham[1], C.C. Klepper[9], A. Meigs[1], D. Milanesio[10], J. Mlynar[11], T. Pütterich[2], A. Sirinelli[1] and JET EFDA contributors*

JET-EFDA, Culham Science Centre, OX14 3DB, Abingdon, UK

[1]EURATOM-CCFE Fusion Association, Culham Science Centre, OX14 3DB, Abingdon, OXON, UK
[2]Max-Planck-Institut für Plasmaphysik, EURATOM-Assoziation, Garching, Germany
[3]CEA, IRFM, F-13108 Saint-Paul-Lez-Durance, France
[4]Association Euratom-IPPLM, Hery 23, 01-497 Warsaw, Poland
[5]Association EURATOM-Belgian State, ERM-KMS, Brussels, Belgium
[6]EFDA Close Support Unit, Garching, Germany
[7]IEK-4, Forschungszentrum Jülich, Association EURATOM-FZJ, Germany
[8]Ecole Nationale des Ponts et Chaussées, F77455 Marne-la-Vallée, France
[9]Oak Ridge National Laboratory, Oak Ridge, TN 37831-6169, USA
[10]Politecnico di Torino, Department of Electronics, Torino, Italy
[11]Association EURATOM-IPP.CR, Za Slovankou 3, 182 21 Praha 8, Czech Republic
** See annex of F. Romanelli et al, "Overview of JET Results", (24th IAEA Fusion Energy Conference, San Diego, USA (2012)).*

Preprint of Paper to be submitted for publication in
Physics of Plasmas

ABSTRACT.
In 2011/12, JET started operation with its new ITER-Like Wall (ILW) made of a tungsten (W) divertor and a beryllium (Be) main chamber wall. The impact of the new wall materials on the JET Ion Cyclotron Resonance Frequency (ICRF) operation is assessed and some important properties of JET plasmas heated with ICRF are highlighted. A ~20% reduction of the antenna coupling resistance is observed with the ILW as compared with the JET carbon (JET-C) wall. Heat-fluxes on the protecting limiters close the antennas, quantified using Infra-Red (IR) thermography (maximum 4.5 MW/m^2 in current drive phasing), are within the wall power load handling capabilities. A simple RF sheath rectification model using the antenna near-fields calculated with the TOPICA code can reproduce the heat-flux pattern around the antennas. ICRF heating results in larger tungsten and nickel (Ni) contents in the plasma and in a larger core radiation when compared to Neutral Beam Injection (NBI) heating. The location of the tungsten ICRF specific source could not be identified but some experimental observations indicate that main-chamber W components could be an important impurity source: for example, the divertor W influx deduced from spectroscopy is comparable when using RF or NBI at same power and comparable divertor conditions, and Be evaporation in the main chamber results in a strong reduction of the impurity level. In L-mode plasmas, the ICRF specific high-Z impurity content decreased when operating at higher plasma density and when increasing the hydrogen concentration from 5% to 15%. Despite the higher plasma bulk radiation, ICRF exhibited overall good plasma heating efficiency; the power is typically deposited at the plasma centre while the radiation is mainly from the outer part of the plasma bulk. Application of ICRF heating in H-mode plasmas has started, and the beneficial effect of ICRF central electron heating to prevent W accumulation in the plasma core has been observed.

1. INTRODUCTION

In 2011/12, JET started operation with its new ITER-Like Wall [1] made of a tungsten divertor and a beryllium main chamber wall with some recessed W-coated components (e.g. NBI shine-through protection tiles, re-ionisation tiles, restraint ring protections). ICRF heating using the A2 antennas [2] was routinely used to provide central electron heating in support to the experimental program which focused on the characterization of fuel retention with the ILW, characterization of H-mode access and high performance scenario development [3]. Plasma compatibility and performance of ICRF heating (hydrogen minority, deuterium plasma) with the full metallic environment was studied [4]; 5 MW of RF power were launched into L-mode plasmas and up to 4 MW in ELMy H-mode. The main objective of the initial ICRF experiments in JET with the ILW (JET-ILW) was to verify compatibility of the operation with the ILW environment: (a) Verify if the new wall induced a change in the antenna coupling resistance. (b) Characterize ICRF specific heat loads on the Plasma Facing Components (PFCs) in the vicinity of the antennas. (c) Verify if the use of ICRF with the ILW led to an increased level of W impurity in the plasma. (d) Characterize JET plasmas with ICRF heating, from the point of view of heating efficiency and of the effect of central heating on high Z impurity transport.

The JET ICRF heating system includes four "A2" ICRF antennas (A, B, C, and D, see Figure 1). The ITER-Like ICRF antenna (ILA) was not used in 2011/12. Each A2 antenna [2, 5] is a phased array of 4 poloidal straps; controlling the phase between straps allows waves to be launched with different $k_{//}$ spectra. Usually π (dipole phasing) or +/- $\pi/2$ phasing (current drive phasings) between adjacent straps are used. The plasma facing part of the antennas is covered by a Faraday screen consisting of tilted solid Be rods. Each antenna is surrounded by two poloidal limiters made of solid Be tiles, and a vertical septum made of solid Be is fitted at the centre of each antenna. During this campaign, antenna C and D were either fed independently or through an External Conjugate-T arrangement with plasma Edge Localized Mode (ELM) resilience properties [6]; straps 1&2 of antennas A and B were fed by the same RF amplifiers through a 3dB hybrid coupler system [5] also providing ELM resilience. Straps 3&4 of antenna A were fed by independent amplifiers; straps 3&4 of antenna B were not available, consequently only straps 1,2 of antenna A and B could be used on ELMy H-mode plasmas. A numerical model of the A2 antennas has recently been built to be used with the antenna electromagnetic modeling code TOPICA [7] (see Figure 2), the same antenna code is used for the design of the ITER ICRF antenna [8]. TOPICA simulations are now being used to analyze the operation of JET A2 antennas.

2. ANTENNAS OPERATION AND RF/SOL INTERACTION

2.1 ANTENNA LOADING

For a given V_{max}, the maximum operating RF voltage in the antenna structure (or in the ICRF system transmission lines) limited by voltage stand-off, the achievable coupled power varies to a first approximation linearly with the antenna coupling resistance R_c: $P_{Coupled} \sim V^2_{max} R_c / 2 Z^2_c$, where Z_c is the transmission line characteristic impedance ($Z_c = 30\Omega$ for JET ICRF transmission lines). The antenna coupling resistance *Rc* is expected to decrease exponentially with the distance between the antenna and the fast wave density cut-off position [9], the cut-off density being typically in the range [1-5]10^{18} m^{-3} for JET operating parameters. A statistical analysis of *Rc* has been carried-out to verify whether if the change to a low recycling wall (the ILW) has led to changes in the Scrappe-Off Layer (SOL) properties which affect the ICRF antenna coupling resistance. The result is shown in Figure 3 for antenna A. *Rc* is plotted as a function of the averaged plasma-outer limiter distance over the antenna straps height. The data set includes L-mode pulses with low triangularity, B_T in the range [2.35-2.9] Tesla, I_P in the range [1.8-2.5] MA, the line integrated density in the range [5-6.5] $10^{19} m^{-2}$. The operating frequency is 42.56MHz and the strap phasing is 'dipole'. The coupling resistance is averaged over the operating straps. One can note that the coupling resistance decreases approximately exponentially with the plasma-outer limiter distance as expected. The scatter in the JET-C data is larger, this is attributed to the fact that the JET-C data-set includes pulses with a wider range of operating conditions that can affect the SOL conditions in particular different divertor configurations with the outer strike point either on tile 5, 6 or 7 (see Figure 1). On the contrary, the JET-ILW dataset includes almost exclusively plasmas with the strike point on tile 5.

For equivalent plasma outer limiter distance, plasma shape and plasma density, the A2 antennas

coupling resistance in JET-ILW is slightly reduced (by ~ 20% at most) as compared with JET-C, which is equivalent to an inward shift of the cut-off layer of ~1cm; this could be a consequence from the change in the wall recycling properties, although no obvious differences were observed comparing JET-C and JET-ILW SOL measurements [10]. The slightly improved coupling with the JET-C could be a consequence of local changes in the SOL properties in front of the powered antennas from the local recycled gas as was observed in ICRF coupling improvement via local gas puffing experiments in ASDEX-Upgrade [11] and JET [12]. Finally one could not rule out the possible introduction of a systematic error of the order of one cm in the localization of the separatrix position from plasma equilibrium reconstruction when going from JET-C to JET-ILW.

Preliminary results for the analysis of the A2 antennas *Rc* measurements using TOPICA, are presented in Figure 4**.** For a series of JET-ILW L-mode pulses where the plasma mid-plane outer gap was changed, *Rc* from antenna A is compared to the calculations from TOPICA; in these cases only straps 1&2 were used. The plasma temperature and density profiles representative of the profiles in the L-mode discharges have been loaded in TOPICA simulations. For dipole phasing, the simulations reproduce well the measured coupling resistance dependence with antenna-plasma distance. For -π/2 phasing, the measured coupling resistance is higher as compared to dipole, this behavior is also reproduced in TOPICA simulations. The error bar in Figure 4 corresponds to the uncertainty in the absolute radial position of the SOL density profiles measured in JET (from the reflectometry diagnostic or Lithium-beam diagnostic). Further analysis is ongoing to study cases with the 4 antenna straps powered, providing a further and sound validation of this numerical tool.

2.2 ICRF SPECIFIC HEAT LOADS ON ANTENNA LIMITERS

When using ICRF heating, local hot spots from enhanced heat-fluxes are commonly observed on some plasma facing components close to the antennas [13], an example is shown in Figure 5. Experiments have been carried out during the initial experimental campaign with the JET-ILW to characterize the heat flux to the A2 antenna limiters [14]. Using IR thermography and thermal models of the tiles, heat-fluxes were evaluated from the surface temperature increase during the RF phase of L-mode plasmas. The maximum observed heat-flux intensity was ~4.5MW/m^2 when operating with –π/2 strap phasing at power level of 2MW per antenna and with a 4cm midplane outer gap ($\Delta T_{surface} = 375^oC$ on antenna A septum during the 5 seconds ICRF phase in JET Pulse No: 81702). The heat-fluxes were enhanced when using current drive phasing; the intensity was found to increase linearly with the density at radial position corresponding to the antenna and with the square of the RF voltage at the antinodes of the transmission lines feeding the antenna. The Be tiles of the A2s protecting limiters can handle fluxes of the order of 6MW/m^2 for 10sec, therefore RF specific heat-fluxes are in practice not a limitation for JET ICRF operation (although hot spots need to be monitored). However, these heat-flux values deserve further attention, in particular when compared to the engineering design targets (5MW/m^2) for the ITER ICRF antenna Faraday screen and neighboring blanket modules.

To optimize the design of the antennas for future devices, modeling activities of ICRF sheath

rectification are carried out within the ICRF community (see for example [15]). We have tested a simple RF sheath rectification model in particular to verify if the intensity and the location of the hot-spots measured on the JET antenna protecting limiters is consistent with the $E_{//}$ map in front of the A2s as calculated using the TOPICA code ($E_{//}$ is the RF electric field that drive RF sheath rectification, // denotes the direction parallel to static magnetic field) [16]. In the simplified model derived from [17], $Q_{\|} = e\ Z\ n\ c_s\ V_{DC}$ where e is the elementary charge, Z is the atomic number of plasma ions (D_+), c_s is the ion sound speed in the SOL, n is the electron density at the antenna and $V_{DC} = \frac{1}{2}|E_{\|}\ dl\ |$ is the RF rectified sheath potential. In the model, the reflectometer or lithium-beam density measurements are mapped along the poloidal limiters to estimate the local density. The $E_{//}$ in front of the antenna is from TOPICA modeling. The field is calculated 4.5 mm in front of the limiters; the field intensity is scaled to the launched ICRF power. The integration path to calculate V_{DC} is along the tilted field lines up until the location of the poloidal limiter. A typical result is shown in Figure 6 for Pulse No: 83063 where only strap 3&4 of antenna A were used with $-\pi/2$ phasing. The heat-flux estimated from IR thermography along the 2D poloidal limiter is plotted as a function of the vertical height, and it is compared to the estimates from the simple model; the model can reproduce the vertical location of the maximum heat-flux and the magnitude of the heat-flux within the uncertainty of the density measurements. It is important to take into account the variation of n along the height of the limiter (plasma-limiter distance is not uniform along the limiter, n peaks at ~0.3m) in order for the model to reproduce the location of the maximum load. The model is also consistent with the observed reduced intensity of the hot-spot when the strap phasing is dipole instead of current drive. However the simple model cannot explain the observed experimental scaling of the ICRF specific heat-loads with V^2, more complex phenomena such as the modification of plasma properties in front of the antennas by ICRF power can also be involved explaining this scaling [18].

2.3 ICRF SPECIFIC IMPURITY SOURCE

During ICRF heating, the bulk radiated power is found to increase compared to C-wall operation although not preventing efficient heating of the plasma. The radiated power is noticeably higher when using ICRF instead of NBI heating (see Figure 7 and Figure 9). The main radiators in the plasma bulk are W (new to the JET-ILW) and Ni (which was also observed in JET-C [19]). The plasma Be content is also higher with ICRF heating.

Ni [19] and W [20][21] was detected from Vacuum Ultra Violet (VUV) spectroscopy operating in the range 10-110 nm. Analysis of Soft-X Ray (SXR) signals including a 2D spatial deconvolution of the emission was also used to evaluate the W concentration ($c_{\_W}$) profiles [20] in the plasma. In this case, the Bremstrahlung emission from low Z impurities is subtracted from the SXR signals and it is assumed that W is the only other radiator contributing to SXR emission. Further, the total radiation profiles can be recalculated and compared to the Bolometric measurements (Figure 10).

One could invoke a change in transport of W and Ni in the plasma core during ICRF to explain the enhanced level of impurity when using ICRF, but preliminary transport analysis [22] suggests

that there are also specific ICRF Ni and W sources. It was plausible to suspect that RF sheath rectification along the field lines which connect the powered antennas to the divertor, could enhance W sputtering in the divertor region. ICRF field – SOL interaction could indeed be evidenced [23]; For example, enhanced Be sputtering was observed using Be I or Be II line spectroscopy with line of sight falling on a limiter close to antenna D or on the Faraday Screen in front of strap 4 of antenna D [24]. The effect was enhanced when using -π/2 strap phasing. Also, the W I emission at the outer divertor baffles, measured with an intensified CCD camera fitted with a 1nm filter (centered at 400.9nm), was found to change depending on which specific antenna was powered, the effect in this case also enhanced when using -π/2 phasing which is expected to generate higher V_{DC} that drives RF sheath rectification. The possible mechanisms responsible for enhanced sputtering of W and Ni during RF are: (a) near field RF sheath rectification; (b) far field RF sheath rectification; (c) charge exchanged neutrals of RF accelerated fast particles. However we could not identify the main mechanism at play in JET and we could not directly link the increased W content in the plasma to a specific W source when using ICRF heating. In particular, W line emission spectroscopy [25] did not evidence higher W sputtering in the divertor region when using ICRF heating [23]. The W components located in the main chamber could also contribute importantly to the W in the plasma. In limiter configuration, ICRF heated plasmas also had higher $c_{\_W}$ compared to NBI. Moreover, when in such a limiter discharge the plasma was shifted upwards away from the divertor, providing better magnetic isolation between the divertor and the antennas, $c_{\_W}$ did not decrease. Further we have investigated the effect of covering the wall with a thin layer of Be through an overnight evaporation (see Figure 7). Comparison of reference pulses before/after evaporation (~3 nm thick Be layer) shows a strong reduction of the Ni and W concentration level, and of the bulk radiated power. The effect was still visible after ~10 ELMy H-modes pulses. This is consistent with the idea that Ni and W surfaces on remote areas in the main chambers were screened from sputtering by the Be layer which suggests that these areas contribute significantly to the high Z impurity source in JET.

3. ICRF PLASMA HEATING

3.1 PLASMA PARAMETERS AND HIGH Z IMPURITY CONTENT

The edge density is a key parameter that influences the plasma impurity content, $c_{\_W}$ [23] and $c_{\_Ni}$ [21] being both reduced when operating at higher density. A number of different processes could lead to this result: a) a decrease of the impurity source from a reduced electron temperature in the SOL when operation at higher density (using higher level of gas dosing); b) a change in impurity transport properties; c) a direct dilution of the impurities in the plasma and d) a reduction of the antenna RF field at higher SOL density reducing RF sheath rectification effects.

An experiment was run to investigate the effect of the hydrogen minority concentration on impurity concentration in L-mode plasmas ($B_T = 2.7$ T, $I_p = 2$MA, 42MHz ICRF); working at H concentration of ~ 15% – somewhat higher than the few percents traditionally used for minority heating – caused a reduction of the W and Ni concentration and of the bulk radiation. Impurity concentration and radiated power increased again when the H fraction was increased above 20%.

A tentative explanation for these observations has been proposed in [26]: increasing the hydrogen fraction on one hand increased the edge density; As already mentioned in the previous paragraph, this tends to reduce the plasma impurity content. But it also reduced the wave absorption efficiency in the plasma core which increased the power fraction re-incident on the edge, the latter hindering coupling when the hydrogen fraction was increased above 20%. We should also add that for the pulses with low H concentration, the plasma entered into M-mode (regime with enhanced particle confinement [27]); this change in confinement regime could be involved in the observed changes in the SOL density when varying the H fraction. The effect of the M-mode of the high Z impurity transport at the edge barrier could also not be ruled-out.

3.2 ICRF HEATING EFFICIENCY:

During the initial campaign of JET-ILW, fundamental H minority heating in D plasmas was almost exclusively used, with the cyclotron resonance either on-axis or off-axis. Except for specific experiments reported in the previous paragraph, H_2 was injected to establish a H fraction of ~5%. This heating regime when applied on-axis, leads mainly to power deposition on the bulk electrons by collisions with the ICRF - accelerated H ions, and it generally has good single pass wave absorption. The ICRF heating efficiency was found similar than for JET-C [28][29]. Surprisingly, as is shown in Figure 8 the plasma energy achieved per MW of ICRF power has only slightly reduced with respect to the JET-C, despite the significantly higher bulk radiation level observed with the JET-ILW. The plasma heating capabilities of NBI and ICRF waves were also found similar [30] [31]. The heating performance of ICRF waves is further illustrated in Figure 9 and Figure 10 from [31]. Pulse No: 81852 is a L-mode plasma ($B_t = 2.55T$, $I_p = 2MA$, $n_{e,0} = 2.4\times10^{19}m^{-3}$) with a ICRF phase ($f = 42MHz$) and a NBI phase (3.5MW input power in both cases); despite the larger W and Ni impurity content during RF which explains the larger radiated power in the plasma bulk (1.5 larger), the plasma thermal energy is similar for both phases. Two important factors contribute in preserving the overall ICRF heating performance. First, ICRF waves heat efficiently the electrons in the plasma centre as shown from the central electron temperature increase (Figure 9-b). Second, plasma radiates power mainly from the outer part as is shown in Figure 10 from bolometric signals and SXR signals analysis. During the RF phase, less than 20% of the total radiated power comes from $\rho < 0.4$ and less than 3% from $\rho < 0.15$.

3.3 USE OF ICRF HEATING IN H-MODE PLASMAS

H-mode plasmas with the JET-ILW are prone to W accumulation if reducing the gas dosing too much [3]; indeed, a higher level of gas injection contributes to increase the ELM frequency and reduce the intensity of impurities source. But it also affects the plasma energy confinement [32]. Central electron heating was proved efficient on ASDEX-Upgrade to increase local transport of high Z impurities and prevent accumulation [33]. Although ICRF heating was used in the H-mode plasmas only late in the initial JET-ILW experimental campaign, we have indications that this tool can be used in JET-ILW to prevent impurity accumulation. This is pictured in figures 11, 12 and 13

for Pulse No: 83897 ($B_t = 2.65$ T, $I_p = 22$MA, 16.0MW NBI) and Pulse No: 83603 (same plasma, 14.4MW NBI and 3.4MW ICRF heating). Due to the slightly lower NBI power in 83603, the ELM are less frequent before the ICRF phase and impurity flushing by the ELMs at the edge transport barrier is less efficient, hence the increased total radiated power for Pulse No: 83603 at the beginning of the H-mode phase. The central electron temperature (Figure 13-b and Figure 13-d) is higher in Pulse No: 83603 thanks to the efficient central electron ICRF heating. In both pulses, infrequent sawteeth are present (~350ms period in Pulse No: 83597 and ~400ms in Pulse No: 83603). In Pulse No: 83597 the central temperature is decreasing halfway through the sawteeth period, before the crashes, indicating radiating cooling in the plasma centre. This is confirmed by the radiation emission peaked at the centre as measured by bolometry (not shown) and SXR tomography (Figure 12-a). The tungsten concentration in these plasmas was evaluated from the analysis of SXR emission (see section III-A) in [34]. The result is shown in Figure 13-a and Figure 13-c. For the no-RF case, c_W peaks at the centre up to values in the order of 10^{-3}. With ICRF heating in Pulse No: 83603 c_W at mid radius is larger than for NBI heating only, consistent with the overall larger plasma radiation (Figure 11-c), but tungsten peaking in the center is less pronounced, and c_W at the centre even decreases in the second half of the sawtooth cycles. These results illustrate the potential of central ICRF heating to prevent W accumulation in JET-ILW plasmas.

The possible mechanisms for the reduction of tungsten peaking with ICRF heating in these pulses are discussed in [35]. Central heating could enhance outward neo-classical and anomalous W transport. The observed increased fishbone activity during the pulse with ICRF (during the second half of the sawteeth cycles) which coincides with the reduction of c_w at the centre content also indicates that MHD activity could be an underlying cause for the change of tungsten transport.

CONCLUSIONS

We have characterized operation of the ICRF system during the first experimental campaign with the JET-ILW; the ICRF system operation did not encounter limitations due to the change from the carbon wall to the ILW. The A2 antenna loading is slightly decreased, by at most 20%, with the ILW as compared with JET-C when comparing equivalent plasma conditions. ICRF specific heat fluxes at the antennas are within the JET wall heat handling capabilities. In addition, progresses are being made toward the validation of the antenna modeling code TOPICA and of the optimization procedure to reduce the effects of RF sheath rectification in the design of the ITER antenna.

In L-mode, radiation from the JET bulk plasma and impurity levels are higher as compared to NBI, but generally the ICRF heating is efficient and plasma does not exhibit peaked centre radiation. In addition, we have indications that ICRF central heating is efficient in H-mode plasmas to prevent central W accumulation. In the JET campaign starting in summer 2013, more power will be available in H-mode (straps 3,4 from antenna A and B will be available in the ELM resilient configuration). The emphasis will be on the optimization of the use of ICRF heating to prevent W accumulation, using the ICRF capabilities to provide central electron heating and as a tool for MHD activity control [36].

AKNOWLEDGEMENTS

The support from the JET ICRH system group is warmly acknowledged. This work, part-funded by the European Communities under the contracts of Association between EURATOM and CCFE, was carried out within the framework of the European Fusion Development Agreement. The views and opinions expressed herein do not necessarily reflect those of the European Commission. This work was also funded by the RCUK Energy Programme under grant EP/I501045.

REFERENCES

[1]. G.F. Matthews, P. Edwards, T. Hirai, M. Kear, A. Lioure, P. Lomas, A. Loving, C. Lungu, H. Maier, P. Mertens, D. Neilson, R. Neu, J. Pamela, V. Philipps, G. Piazza, V. Riccardo, M. Rubel, C. Ruset, E. Villedieu and M. Way on behalf of the ITER-like Wall Project Team, Physica Scripta **T128** (2007) 137–143

[2]. A. Kaye, T. Brown, V. Bhatnagar, P. Crawley, J. Jacquinot, R. Lobel, J. Plancoulaine, P.-H Rebut, T. Wade, C Walker, Fusion Engineering and Design **24** (1994) 1-21

[3]. R. Neu , G. Arnoux , M. Beurskens , V. Bobkov , S. Brezinsek , J. Bucalossi , G. Calabro, C. Challis , J. W. Coenen , E. de la Luna , P. C. de Vries , R. Dux , L. Frassinetti , C. Giroud , M. Groth , J. Hobirk , E. Joffrin , P. Lang , M. Lehnen , E. Lerche , T. Loarer , P. Lomas , G. Maddison , C. Maggi , G. Matthews , S. Marsen , M.-L. Mayoral , A. Meigs , Ph. Mertens , I. Nunes , V. Philipps , T. Pütterich , F. Rimini , M. Sertoli , B. Sieglin , A. C. C. Sips , D. van Eester , G. van Rooij and JET-EFDA Contributors, Physics of Plasmas **20**, 056111 (2013)

[4]. M.-L. Mayoral, V. Bobkov, A. Czarnecka, I. Day, A. Ekedahl, P. Jacquet, M. Goniche, R. King, K. Kirov, E. Lerche, J. Mailloux, D. Van Eester, O. Asunta, C. Challis, D. Ciric, J.W. Coenen, L. Colas, M.C. Giroud, M. Graham, I. Jenkins, E. Joffrin, T. Jones, D. King, V. Kiptily, C.C. Klepper, C. Maggi, F. Marcotte, G. Matthews, D. Milanesio, I. Monakhov, M. Nightingale, R. Neu, J. Ongena, T. Pütterich, V. Riccardo, F. Rimini, J. Strachan, E. Surrey, V. Thompson, G. Van Rooij and JET EFDA contributors, On the challenge of plasma heating with the JET metallic wall, in Proceedings of 24th IAEA Fusion Energy Conference (San Diego, USA, 2012), EX/4-3

[5]. M. Graham, M-L Mayoral, I. Monakhov, J. Ongena, T. Blackman, M.P.S. Nightingale, E. Wooldridge, F. Durodié, A. Argouarch, G. Berger-By, A. Czarnecka, S. Dowson, R. Goulding, S. Huygen, P. Jacquet, T.J. Wade, E. Lerche, P.U. Lamalle, H. Sheikh, D. Van Eester, M Vrancken, A Walden, A Whitehurst and JET-EFDA contributors, Plasma Physics and Controlled Fusion **54** (2012) 074011 (11pp)

[6]. I. Monakhov, M. Graham, T. Blackman, S. Dowson, F. Durodie, P. Jacquet, J. Lehmann, M.-L. Mayoral, M.P.S. Nightingale, C. Noble, H. Sheikh, M. Vrancken, A. Walden, A. Whitehurst, E. Wooldridge and JET-EFDA Contributors, Nuclear Fusion **53** (2013) 083013 (21pp)

[7]. D. Milanesio, O. Meneghini, V. Lancellotti, R. Maggiora and G. Vecchi, Nuclear Fusion **49** 115019 (2009)

[8]. F. Durodie, M. Vrancken, R. Bamber, P. Dumortier, D. Hancock, S. Huygen, D. Lockley, F. Louche, R. Maggiora, D. Milanesio, A. Messiaen, M.P.S. Nightingale, M. Shannon, P.

Tigwell, M. Van Schoor, D. Wilson, K. Winkler and CYCLE Team, RF Optimization of the Port Plug Layout and Performance Assessment of the ITER ICRF Antenna, Proc. of the 24th IAEA Fusion Energy Conference (San Diego, USA) ITR/P1-08 (2012)

[9]. Bilato R., Brambilla M., Hartmann D.A. and Parisot A, 2005 Nuclear Fusion **45** L5–7

[10]. M. Groth, S. Brezinsek, P. Belo, M.N.A. Beurskens, M. Brix, M. Clever, J.W. Coenen, C. Corrigan, T. Eich, J. Flanagan, C. Guillemaut, C. Giroud, D. Harting, A. Huber, S. Jachmich, U. Kruezi, K.D. Lawson, M. Lehnen, C. Lowry, C.F. Maggi, S. Marsen, A.G. Meigs, R.A. Pitts, G. Sergienko, B. Sieglin, C. Silva, A. Sirinelli, M.F. Stamp, G.J. van Rooij, S. Wiesen and the JET-EFDA Contributors, Nuclear Fusion **53** (2013) 093016 (11pp)

[11]. P. Jacquet, V. Bobkov, M.-L. Mayoral, I. Monakhov, J.M. Noterdaeme, A. Scarabosio, I. Stepanov, M. Vrancken, E. Wolfrum and the ASDEX Upgrade Team, Nuclear Fusion **52** (2012) 042002 (6pp)

[12]. M.-L. Mayoral, V. Bobkov, L. Colas, M. Goniche, J. Hosea, J.G. Kwak, R. Pinsker, S. Moriyama, S. Wukitch, F.W. Baity, S. Carpentier-Chouchana, A. Czarnecka, A. Ekedahl, G. Hanson, P. Jacquet, P. Lamalle, I. Monakhov, M. Murakami, A. Nagy, M. Nightingale, J.-M. Noterdaeme, J. Ongena, P.M. Ryan, M. Vrancken, J.R. Wilson, EFDA –JET contributors, ASDEX Upgrade team and the ITPA «Integrated Operation Scenarios» members and experts, 2010, On Maximizing the ICRF Antenna Loading for ITER plasmas Proc. Of the 23rd IAEA Fusion Energy Conference ITR/P1-11 http://www-naweb.iaea.org/napc/physics/FEC/FEC2010/html/node54.htm

[13]. P. Jacquet, L. Colas, M.-L. Mayoral, G. Arnoux, V. Bobkov, M. Brix, P. Coad, A. Czarnecka, D. Dodt, F. Durodie, A. Ekedahl, D. Frigione, M. Fursdon, E. Gauthier, M. Goniche, M. Graham, E. Joffrin, A. Korotkov, E. Lerche, J. Mailloux, I. Monakhov, C. Noble, J. Ongena, V. Petrzilka, C. Portafaix, F. Rimini, A. Sirinelli, V. Riccardo, Z. Vizvary, A. Widdowson, K.-D. Zastrow and JET EFDA Contributors, Nuclear Fusion **51** (2011) 103018 (16pp)

[14]. P. Jacquet, F. Marcotte, L. Colas, G. Arnoux, V. Bobkov, Y. Corre, S. Devaux, J.-L. Gardarein, E. Gauthier, M. Graham, E. Lerche, M.-L. Mayoral, I. Monakhov, F. Rimini, A. Sirinelli, D. Van Eester, JET EFDA contributors, Journal of Nuclear Materials **438** (2013) S379–S383

[15]. J. Jacquot, D. Milanesio, L. Colas, Y. Corre, M. Goniche, J. Gunn, S. Heuraux, M. Kubič, Radio-frequency sheaths physics: Experimental characterization on Tore Supra and related self-consistent modelling", proc. 20th topical conf. RF power in plasmas, Sorrento 2013, I3.7, submitted to Physics of Plasmas

[16]. AL. Campergue, P. Jacquet, V. Bobkov, D. Milanesio, I. Monakhov, L. Colas, G. Arnoux, M. Brix, A. Sirinelli and JET-EFDA Contributors, Characterization of local heat flux around ICRF antennas on JET, proceedings of the 20th topical conference on RF power in plasmas, Sorrento, Italy (2013)

[17]. L. Colas, D. Milanesio, E. Faudot, M. Goniche and A. Loarte, Journal of Nuclear Materials **390–391** (2009) 959–962

[18]. M. Becoulet, L. Colas, S. Pecoul, J. Gunn, Ph. Ghendrih, A. Becoulet, and S. Heuraux, 2002 Physics of Plasmas **9** 2619–32

[19]. A. Czarnecka, F. Durodié, A.C.A. Figueiredo, K.D. Lawson, E. Lerche, M-L Mayoral, J. Ongena, D. Van Eester, K-D Zastrow, V.V. Bobkov, I.H. Coffey, L. Colas, P. Jacquet, I. Monakhov and JET-EFDA contributors, 2012 Plasma Physics and Controlled Fusion **54** 074013

[20]. T. Pütterich, R Dux, M.N.A. Beurskens , V. Bobkov, S. Brezinsek, J. Bucalossi, J.W. Coenen, I. Coffey, A. Czarnecka, C. Giroud, E. Joffrin, K.D. Lawson , M. Lehnen, E. de la Luna, J. Mailloux, S. Marsen, M.-L. Mayoral, A Meigs, R. Neu, F. Rimini, M. Sertoli, M. Stamp, G. van Rooij and JET EFDA Contributors, Tungsten screening and impurity control in JET, in Proceedings of 24th IAEA Fusion Energy Conference (San Diego, USA, 2012), pp. EX/P3–15

[21]. A. Czarnecka, V. Bobkov, I. H. Coffey, L. Colas, P. Jacquet, K. D. Lawson, E. Lerche, C. Maggi, M.-L. Mayoral, T. Pütterich, D. Van Eester, and JET-EFDA contributors, Spectroscopic Investigation of Heavy Impurity Behaviour During ICRH with the JET ITER-Like Wall, proceedings of the 20th topical conference on RF power in plasmas, Sorrento, Italy (2013)

[22]. D. Kalupin, I. Ivanova-Stanik, I. Voitsekhovitch, J. Ferreira, D. Coster, L.L. Alves, Th. Aniel, J.F Artaud, V. Basiuk, João P.S. Bizarro, R. Coelho, A. Czarnecka, Ph. Huynh, A. Figueiredo, J. Garcia, L. Garzotti, F. Imbeaux, F. Köchl, M.F. Nave, G. Pereverzev, O. Sauter, B.D. Scott, R. Stankiewicz, P. Strand, ITM-TF contributors and JET-EFDA Contributors, Nuclear Fusion **53** (2013) 123007 (8pp)

[23]. Vl. Bobkov, G. Arnoux, S. Brezinsek, J.W. Coenen, L. Colas, M. Clever, A. Czarnecka, F. Braun, R. Dux, A. Huber, P. Jacquet, C. Klepper, E. Lerche, C. Maggi, F. Marcotte, M. Maslov , G. Matthews, M.L. Mayoral, K. McCormick, A. Meigs, D. Milanesio, I. Monakhov, R. Neu, J.-M. Noterdaeme, Th. Pütterich, F. Rimini, G. Van Rooj, G. Sergienko, D. Van Eester, JET EFDA contributors, Journal of Nuclear Materials **438** (2013) S160–S165

[24]. C.C. Klepper, P. Jacquet, V. Bobkov, L. Colas, T.M. Biewer, D. Borodin, A. Czarnecka, C. Giroud, E. Lerche, V. Martin, M.-L. Mayoral, F. Rimini, G. Sergienko, D. Van Eester, JET EFDA contributors, Journal of Nuclear Materials **438** (2013) S594–S598

[25]. A.G. Meigs, S. Brezinsek, M. Clever, A. Huber, S. Marsen, C. Nicholas, M. Stamp, K.-D. Zastrow, JET EFDA Contributors, Journal of Nuclear Materials **438** (2013) S607–S611

[26]. D. Van Eester, E. Lerche, P. Jacquet, V. Bobkov, A. Czarnecka, J.W. Coenen, L. Colas, K. Crombé, M. Graham, S. Jachmich, E. Joffrin, C.C. Klepper, V. Kiptily, M. Lehnen, C. Maggi, F. Marcotte, G. Matthews, M.-L. Mayoral, K. Mc Cormick, I. Monakhov, M.F.F. Nave, R. Neu, C. Noble, J. Ongena, T. Pütterich, F. Rimini, E. R. Solano, G. van Rooij and JET-EFDA contributors, Hydrogen minority ion cyclotron resonance heating in presence of the ITER-Like Wall in JET, proceedings of the 20th topical conference on RF power in plasmas, Sorrento, Italy (2013)

[27]. Emilia R. Solano, F. Rimini, B. Alper, P. Belo, A. Boboc, M. Brix, A. Figueiredo, L. Frassinetti, S. Gerasimov, D. Howell, C. Maggi, K. McCormick, I. Nunes, S. Pinches, D. Refy, B. Sieglin, and JET EFDA Contributors, M-mode: axi-symmetric magnetic oscillation and ELM-less H-mode in JET, Proc. 39th EPS Conference & 16th Int. Congress on Plasma Physics P2.060 (2012)

[28]. D. Van Eester, E. Lerche, P. Jacquet, V. Bobkov, A. Czarnecka, J.W. Coenen, L. Colas, K.

Crombé, M. Graham, S. Jachmich, E. Joffrin, C.C. Klepper, F. Marcotte, M.-L. Mayoral, I. Monakhov, F. Nave, J. Ongena, T. Pütterich, F. Rimini, G. van Rooij and JET-EFDA contributors, Characterization of Ion Cyclotron Resonance Heating in presence of the ITER-like wall in JET Proc. 39th EPS Conference & 16th Int. Congress on Plasma Physics P1.094 (2012)

[29]. E. Lerche, D. Van Eester, P. Jacquet, M.-L. Mayoral, V. Bobkov, L. Colas, A. Czarnecka, K. Crombé, I. Monakhov, F. Rimini, M. Santala and JET-EFDA Contributors, Impact of minority concentration on fundamental (H)D ICRF heating performance in JET-ILW, to be submitted to Nuclear Fusion

[30]. E. Lerche, D. Van Eester, Ph. Jacquet, M.-L. Mayoral, V. Bobkov, L. Colas, A. Czarnecka, M. Graham, G. Matthews, I. Monakhov, R. Neu, T. Puetterich, F. Rimini, P. de Vries and JET-EFDA Contributors, Statistical analysis of the ICRF and NBI heating performances in L-mode, proceedings of the 20th topical conference on RF power in plasmas, Sorrento, Italy (2013)

[31]. M.-L. Mayoral, T. Pütterich, P. Jacquet, E. Lerche, D. Van-Eester, V. Bobkov, C. Bourdelle, L. Colas, A. Czarnecka, J. Mlynar, R. Neu and JET-EFDA Contributors, Comparison of ICRF and NBI Heated Plasmas Performances in the JET ITER-Like Wall, proceedings of the 20th topical conference on RF power in plasmas, Sorrento, Italy (2013)

[32]. G. Saibene, L.D. Horton, R. Sartori, B. Balet, S. Clement, G.D. Conway, J.G. Cordey, H.P.L. De Esch, L.C. Ingesson, J. Lingertat, R.D. Monk, V.V. Parail, R.J. Smith, A. Taroni, K. Thomsen and M.G. von Hellermann, 1999 Nuclear Fusion **39** 1133–56

[33]. C. Angioni, L. Carraro, T. Dannert, N. Dubuit, R. Dux -, C. Fuchs, X. Garbet, L. Garzotti, C. Giroud, R. Guirlet, F. Jenko, O.J. W. F. Kardaun, L. Lauro-Taroni , P. Mantica, M. Maslov, V. Naulin, R. Neu, A.G. Peeters, G. Pereverzev, M. E. Puiatti , T. Pütterich, J. Stober , M. Valovič, M. Valisa, H. Weisen, A. Zabolotsky, ASDEX Upgrade Team and JET EFDA Contributors, Physics Plasmas **14** (2007) 055905

[34]. T. Pütterich, R. Dux, R. Neu, M. Bernert, M.N.A. Beurskens , V. Bobkov, S. Brezinsek, C. Challis2, J.W. Coenen, I. Coffey, A. Czarnecka, C. Giroud, A. Gude, E. Joffrin, A. Kallenbach, M. Lehnen, E. Lerche, E. de la Luna, S. Marsen, G. Matthews, M.-L. Mayoral, R.M. McDermott, A. Meigs, M. Sertoli, G. van Rooij, J. Schweinzer the ASDEX Upgrade Team and JET EFDA Contributors, Taming Tungsten in JET and ASDEX Upgrade, 40th EPS conference on Plasma Physics, Espoo, Finland (2013)

[35]. T. Pütterich, R. Dux, R. Neu, M. Bernert, M.N.A. Beurskens , V. Bobkov, S. Brezinsek, C. Challis, J.W. Coenen, I. Coffey, A. Czarnecka, C. Giroud, P. Jacquet, E. Joffrin, A. Kallenbach, M. Lehnen, E. Lerche, E. de la Luna, S. Marsen, G. Matthews, M.-L. Mayoral, R.M. McDermott, A. Meigs, J. Mlynar, M. Sertoli, G. van Rooij, the ASDEX Upgrade Team and JET EFDA Contributors, Observations on the W-transport in the Core Plasma of JET and ASDEX Upgrade, Submitted to Plasma Physics and Controlled Fusion

[36]. J.P. Graves, I.T. Chapman, S. Coda, M. Lennholm, M. Albergante and M. Jucker, (2012) Nature Communications 3, 624 doi:10.1038/ncomms1622

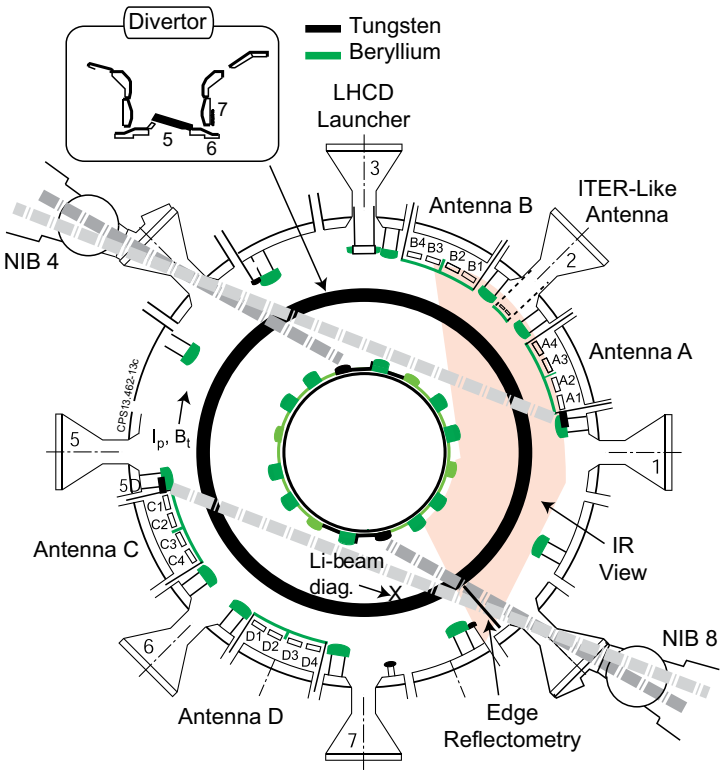

Figure 1: Top view of JET, showing the JET ICRF antennas (A, B, C, D). The view from the IR camera looking at antenna A and B is indicated. Also shown is the position of the reflectometry and Lithium-beam SOL diagnostics. Elements with tungsten surfaces are in black.

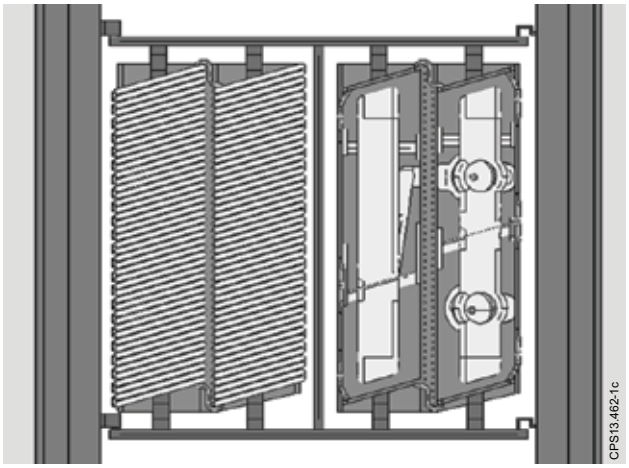

Figure 2: Representation of the JET A2 Antenna TOPICA model. The screen bars were removed from the model representation on the right to illustrate the strap geometry.

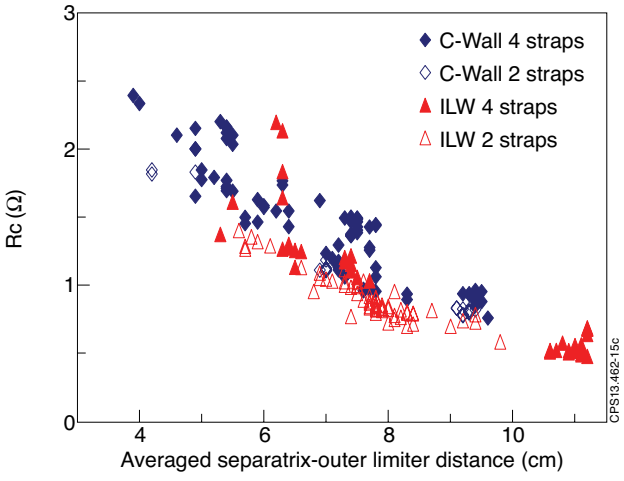

Figure 3: For antenna A, the coupling resistance plotted as a function of the averaged separatrix –outer limiter distance over the height of the antenna straps. The data set includes JET-C and JET-ILW plasmas with low triangularity, and line integrated density in the range [5-6.5]10^{19} m^{-2}. Antenna phasing is dipole, and the operating frequency is 42.56MHz. Operation with all 4 antenna straps are represented with solid symbols (data from the 2013 restart with the JET-ILW are included), operation with straps 1 and 2 only are represented with open symbols.

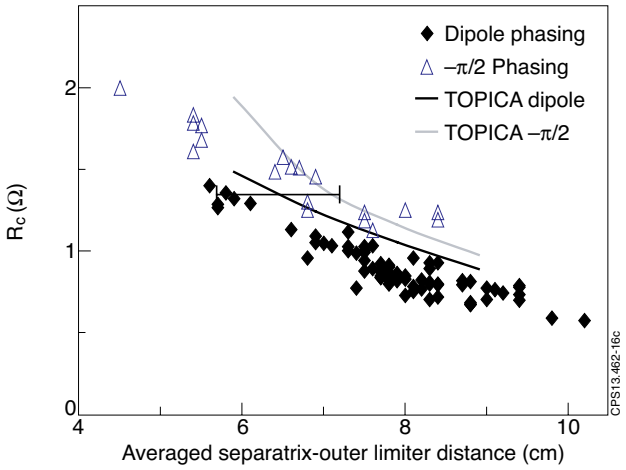

Figure 4: Antenna A coupling resistance measured in JET-ILW and results from TOPICA simulations. Only straps 1&2 are powered. The data set includes plasmas of similar shapes with line integrated density in the range [5-6.5] 10^{19} m^{-2}.

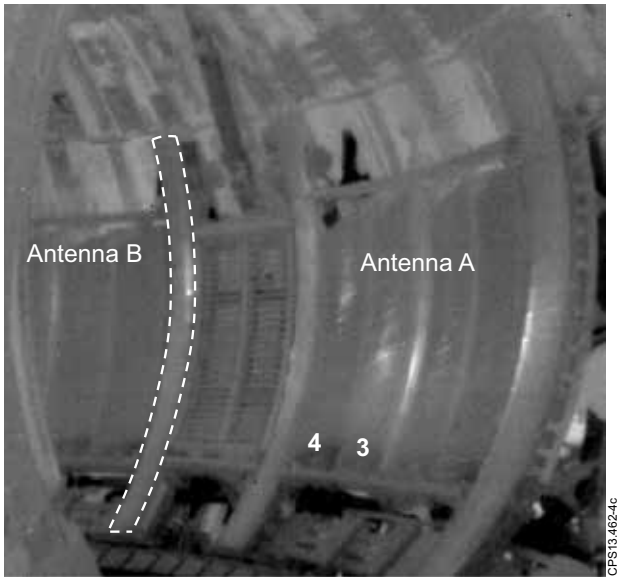

Figure 5: Pulse No: 83063 t=13.0s, IR camera frame showing ICRF hot spots when antenna A (straps 3,4) is powered. The heat-flux on the limiter highlighted with dotted lines is analyzed in Figure 6.

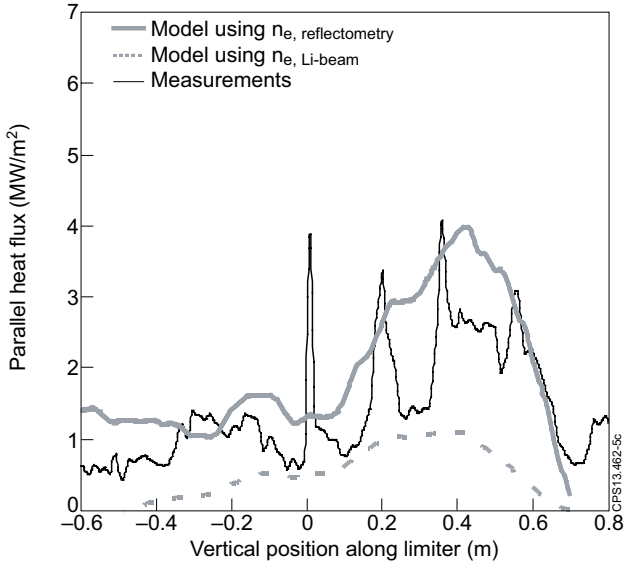

Figure 6: Pulse No: 83603, t=13s, comparison between the heat-flux measured along the poloidal limiter and results from the simple model.

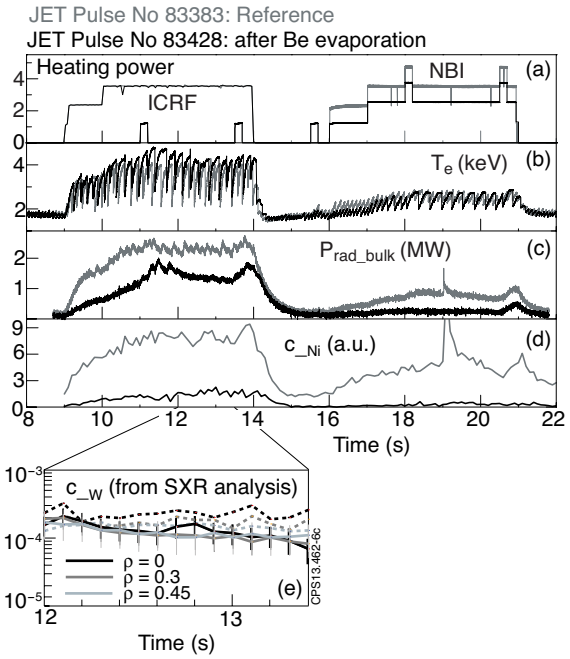

Figure 7: For Pulse No's: 83383 (before Be evaporation, in grey) and 83428 (after evaporation, in black) time trace of (a) ICRF and NBI power, (b) T_e at plasma centre, (c) core radiated power from bolometry and (d) Ni concentration evaluated from VUV spectroscopy. In (e), W concentration evaluated from SXR analysis at different normalized radius is shown (Pulse No: 83383 with dashed lines).

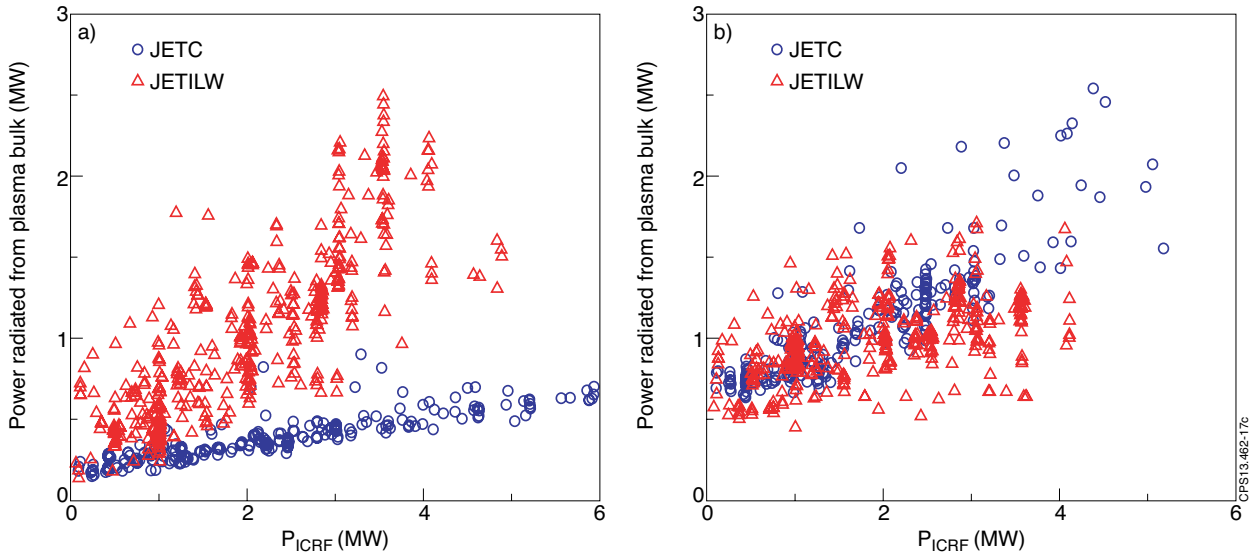

Figure 8: For a database of JET-C and JET-ILW pulses comparison of: (a) power radiated from bulk plasma, from bolometry diagnostic; (b) Plasma thermal energy evaluated from the High-resolution Thomson diagnostic assuming equal electron and ion temperatures. The database includes pulses with ICRF frequency=42MHz, dipole antenna strap phasing, 2.55T<B_T<2.8 T (central heating), line integrated density in the range [5-12]10^{19} m^{-2}.

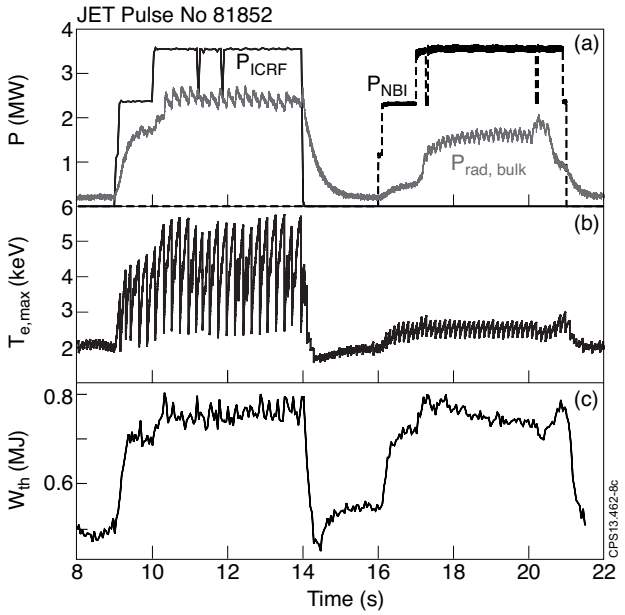

Figure 9: For Pulse No: 81852, (a) time trace of ICRF and NBI power and power radiated in core plasma (grey line); (b) central electron temperature; (c) Thermal energy.

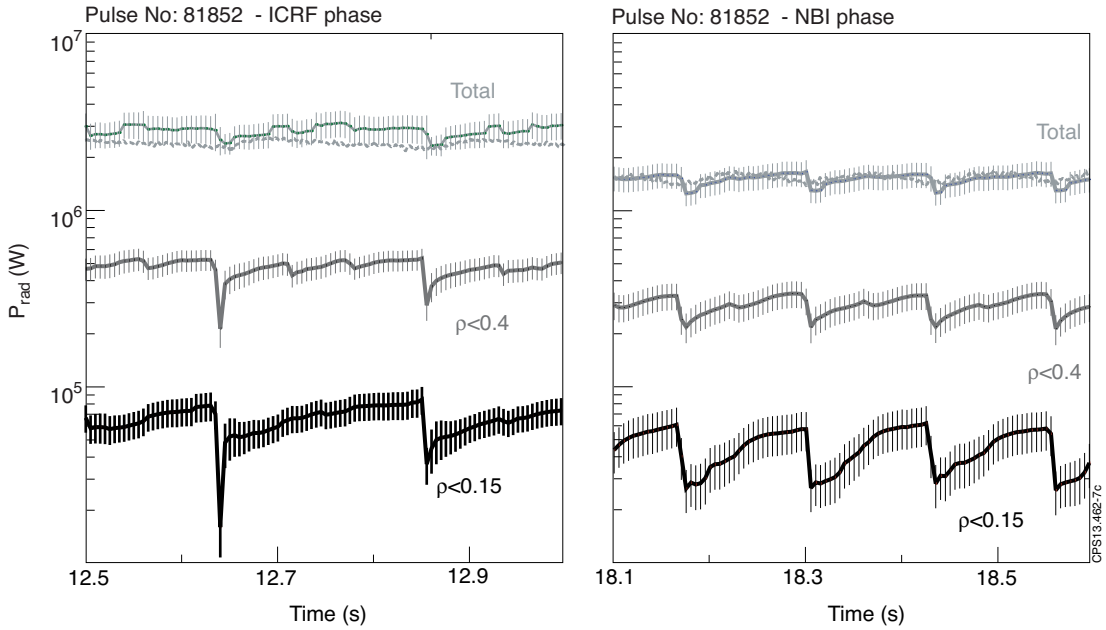

Figure 10: Radiated power (from bolometry and SXR analysis) during the ICRF and NBI phase for Pulse No: 81852; total from plasma bulk (light grey), radiated inside normalized radius (ρ) of 0.4 (grey) and inside ρ=0.15 (black).

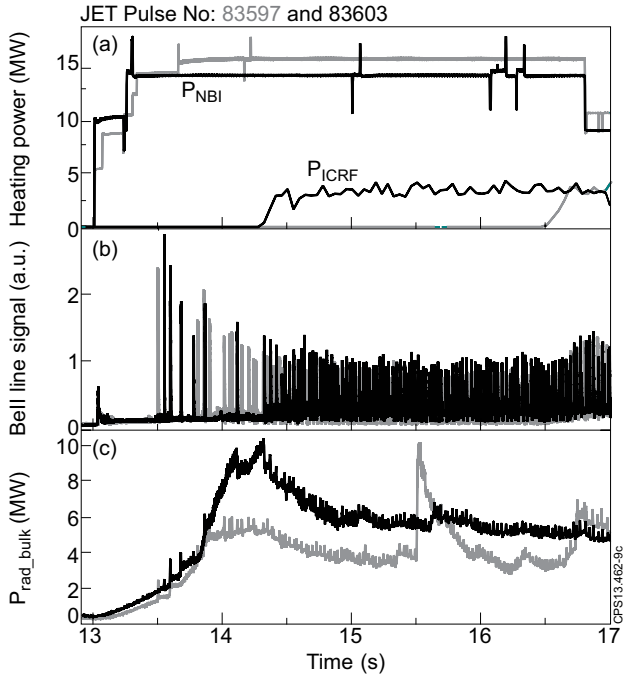

Figure 11: For Pulse No: 83603 (black) and 83597 (grey) traces of (a) heating power, (b) Be II line emission (ELMs) and (c) bulk radiated power.

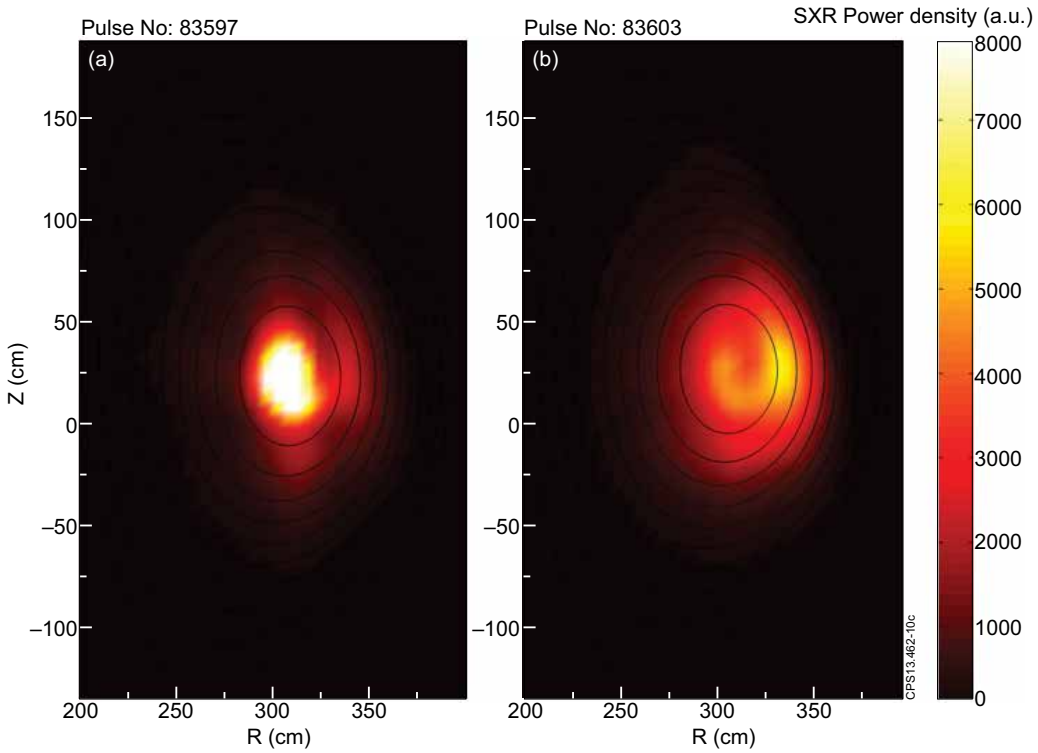

Figure 12: Tomographic reconstruction of SXR emission right before a sawtooth crash: (a) Pulse No: 83597 (NBI only) t = 15.3151s, and (b) Pulse No: 83603 (NBI+ICRF) t = 15.3451s. SXR data are averaged over 10ms.

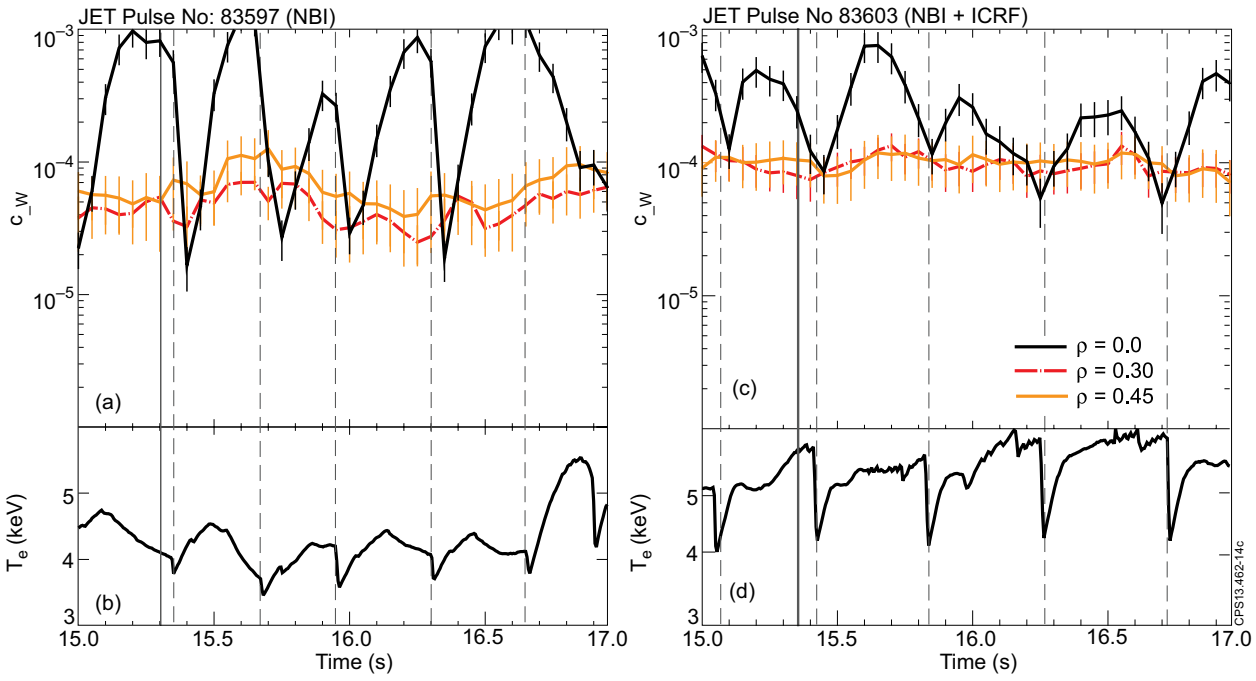

Figure 13: For Pulse No: 83597 with no ICRF, (a) W concentration estimated from SXR emission profile at normalized radius ρ = 0.0, ρ = 0.3 and ρ = 0.45 and (b) T_e at plasma centre. The same quantities are plotted for the Pulse No: 83603 with ICRF in (c) and (d) respectively. The vertical solid lines indicate time when SXR emission profiles are plotted in Figure 12.